Soils and Foundations 2012;52(2):216–227

The Japanese Geotechnical Society

Soils and Foundations

www.sciencedirect.com
journal homepage: www.elsevier.com/locate/sandf

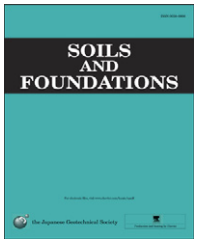

An analytical drilling model of drag bits for evaluation of rock strength

Zhantao Li[a,b], Ken-ichi Itakura[b,*]

[a]*Ningbo University of Technology, Ningbo, China*
[b]*Muroran Institute of Technology, Muroran, Japan*

Available online 29 March 2012

Abstract

To evaluate the unconfined compressive strength (*UCS*) of rocks from drilling data is a promising in-situ method and has been studied by many researchers. In most studies, experimental methods have been used to determine the relationship between *UCS* and drilling data. In this paper, an analytical model is proposed to describe rock drilling processes using drag bits and rotary drills, and to deduce the relations among rock properties, bit shapes, and drilling parameters (rotary speed, thrust, torque, and stroke). In this model, a drilling process is divided into cycles, each of which includes two motions: feeding and cutting. Feeding is treated as an indentation motion. There is a linear relation between indentation pressure (thrust) and the indentation depth (penetration rate). The cutting forces and friction forces of both the rake surface and the flank surface are examined. Also, a virtual base is set to the model to simulate the contact surface between the flank surface of the bit and the rock.

According to this model, drilling torque consists of four parts respectively generated from cutting, friction, feeding, and idle running. Torque caused by friction and idle running is ineffective for drilling, whereas that caused by cutting and indentation is effective. Similar to torque, specific energy also has four parts respectively from cutting, friction, feeding, and idle running. For the purposes of this study, effective specific energy is defined as the sum of specific energy consumed by cutting and feeding. Effective specific energy is independent of the penetration rate. Since it is proportional to the *UCS* of the rocks, it is not influenced by the penetration rate, and is more useful in the evaluation of *UCS* than other parameters. Some laboratory and field tests were conducted, and the results verified the usefulness and effectiveness of the proposed model.

Keywords: Unconfined compression strength; Drilling; Rock cutting theory; Bit wear; Indentation; Effective specific energy (IGC: F00, G14)

1. Introduction

The unconfined compressive strength (*UCS*) of rocks is important in the design and construction of tunnels and coal mines. The measurement of *UCS* is a costly and time-consuming task, because high-accuracy rock specimens are required. Therefore, some in-situ methods to evaluate *UCS* have been proposed in recent years. One of these methods is to evaluate *UCS* from drilling data using a measurement-while-drilling system (MWD). For this evaluation task, it is necessary to conclude the relationship between the *UCS* and the drilling data. Up to now, most studies have used experimental methods to conclude empirical equations. Typically, *UCS* tests for rock specimens are performed in the laboratory and drilling data are recorded and calculated. Then a regression analysis is used to correlate the *UCS* with the drilling data (for example: Teale, 1965; Hoberock and Bratcher, 1996; Finfinger et al., 2000; Kahraman et al., 2003). Rather than a regression analysis, other studies have used neural networks to conclude the relations (for example: Utt, 1999; LaBelle

*Corresponding author.
E-mail addresses: lzt2002@gmail.com (Z. Li), itakura@mmm.muroran-it.ac.jp (K. Itakura).

Peer review under responsibility of The Japanese Geotechnical Society
doi:10.1016/j.sandf.2012.02.002

Notations and abbreviations

ϕ_j	friction angle between the bit and rock (°)
ϕ_i	angle of the internal friction of the rock (°)
β	blade angle of the bit (°)
ψ	angle between the free plane and the failure plane (°)
P	total circumferential force when drilling (N/unit width)
F	thrust when drilling (N/unit width)
F_1	cutting force on the rake surface of the bit (N/unit width)
P_1	main cutting force on the rake surface of the bit (N/unit width)
Q_1	back cutting force on the rake surface of the bit (N/unit width)
P_c	main component of the total cutting force (N/unit width)
Q_c	back components of the total cutting force (N/unit width)
F_2	cutting force on the flank surface of the bit (N/unit width)
P_2	main cutting force on the flank surface of the bit (N/unit width)
Q_2	back cutting force on the flank surface of the bit (N/unit width)
Q_f	load for indentation (N/unit width)
P_f	friction force resulting from the indentation of the bit (N/unit width)
T	total torque when drilling (N m)
Te	effective torque when drilling (N m)
T_i	torque generated from the idle running of a drill (N m)
Es	specific energy when drilling (MJ/m^3)
Ees	effective specific energy (MJ/m^3)
σ	normal stress on the failure plane (Pa/unit width)
τ	shear stress on the failure plane (Pa/unit width)
z	penetration per revolution (mm)
b	contact length of the virtual base (mm)
s	step length of a drilling cycle (mm)
h	indentation depth of a drilling cycle (mm)
r	radius of a point at the bit blade (m)
r_1	outer radius of the bit (m)
r_2	inner radius of the bit (m)
n	stress distribution coefficient of the failure plane
A	effective cross-sectional area of the hole (m^2)
q_u	the unconfined compressive strength (MPa)
IM	indentation modulus (kN/mm)
ΔN	change in load (kN)
Δd_i	change in indentation (mm)
IS	indentation strength (MPa/mm)
ΔP	change in pressure (MPa)
UCS	unconfined compressive strength (MPa)
MWD	measurement while drilling

et al., 2000; Gunes et al., 2007; Martin, 2007; Beattie, 2009). However, these experimental methods using either regression analysis or neural networks have not revealed the causes of the relationship between *UCS* and the drilling data. Therefore, the results of these studies differ considerable, and are often contradictory because of the different experimental methods and conditions employed. A theoretical analysis based on rock cutting theories is needed for a consistent solution.

During the last several decades, the emphasis of rock cutting theories has changed from analytical models to numerical models. Despite this, analytical models are capable of elucidating simple relations among cutting forces, rock properties, bit shapes, and mechanical parameters at acceptable accuracies. Therefore, analytical models remain important for the study of cutting processes overall.

Many analytical models for rock cutting have been proposed. Evans (1962) developed a fundamental theory of coal plowing. According to this model, the failure in the direction of the wedge tip is fundamentally attributable tensile forces, and the cutting forces of a wedge-shaped tool penetrating rocks were investigated. Nishimatsu (1972) proposed a rock cutting model similar to Merchant's (1945) metal cutting model. In Nishimatsu's model, brittle failure is induced as a result of shear forces. Roxborough and Philips (1975) developed a cutting model for disk cutters. Nakajima and Kinoshita (1979) presented a rock cutting model in which crack propagation is the failure mode. Goktan (1997) improved Evans's cutting theory for conical bits. Detournay and Defourny (1992) and Detournay et al. (2008) put forward a cutting theory for drag bits and deduced a linear relationship among thrust, torque and the penetration rate.

Among these theories, those developed by Evans and Nishimatsu are the most comprehensive and accepted (for example, Deketh, 1995; Rojek, 2007; Su and Akcin, 2009; Okubo et al., 2010). However, Evans's model is for penetration rather than a cutting model. Different from penetrating in Evans's model, the flank angle of the tool in Nishimatsu's model is a plus one, just like a lathe tool for metal cutting. Therefore, it can be used to analyze cutting processes by drag bits. Moreover, comparing with other cutting theories, Nishimatsu's model provided simpler relations between cutting forces and rock strength. In this study, Nishimatsu's analytical model of rock cutting was adopted. To allow for fitting to real cutting conditions, a virtual base has been added to Nishimatsu's model. This also makes it possible to analyze the friction on the flank surface of the bit.

It must be pointed out that the above studies are focused on rock cutting rather than drilling. Most researchers treated the drilling process as only a continuous cutting process. In fact, a drilling process contains not only cutting, but also feeding. The latter enables the bit to cut into a new layer. Although many studies in rock cutting have been reported, few analytical models have been developed to describe drilling processes. In this paper, we propose an analytical model of drag bits for rock drilling. This model consists of a series of successive cycles, each of which comprises a cutting motion and a feeding motion.

The feeding motion is in the axial direction of the bit. It is indispensable for a drill process to cutting into new layers of the rocks. A feeding motion perhaps involves indentation, grinding, crushing, and smashing. However, for a small-type drill, a feeding motion can be regarded approximately as an indentation. Here, Mateus et al.'s (2007) theory was used to analyze the cutting forces involved in the feeding operation.

Based on the proposed rock drilling model, several equations have been induced to represent the correlations between the mechanical data and rock properties. Also, a new in-situ method is suggested to evaluate the *UCS* from effective specific energy. Some laboratory and field tests were conducted, and the results verified the correctness of the proposed model and the method for evaluating the *UCS*.

2. Drilling model

We proposed an analytical drilling model as presented in Fig. 1. In this model, the rock is a hollow circular cylinder which has outer and inner diameters equal to those of the drag bit. A drilling process consists of successive cycles, each of which is composed of two motions: cutting and feeding. Herein, Nishimatsu's (1972) model is expanded to analyze rock cutting motions in drilling. Feeding, a complex operation when drilling, can involve indentation, grinding, crushing, and smashing. For small drills, feeding can be treated approximately as indentation. Herein, Mateus's et al. (2007) indentation model is used to analyze feeding forces while drilling.

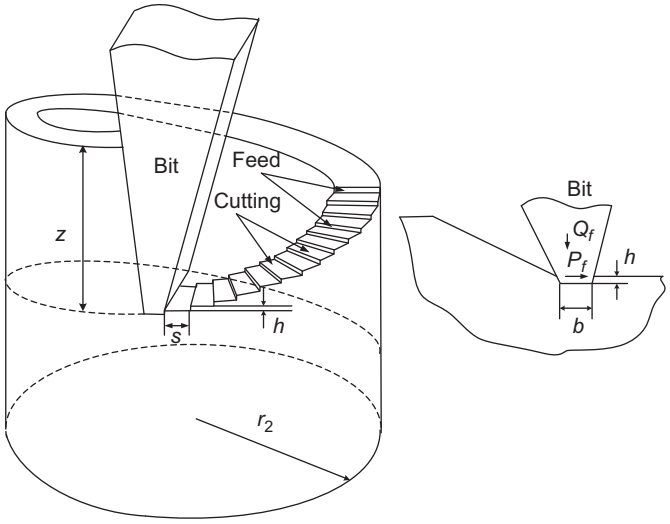

Fig. 1. Cutting and feed movements of a drill bit.

2.1. Cutting motions in a drilling process

We analyzed cutting motions in drilling processes based on Nishimatsu's rock cutting theory. A model of the geometric and mechanical conditions during cutting is presented in Fig. 2. Table 1 presents meanings of the notations used in Fig. 2 and throughout this paper.

The relation between the axial force Q_1 and the circumferential force P_1 can be expressed as

$$\frac{Q_1}{P_1} = \cot(\beta+\phi_j), \tag{1}$$

where, β is the blade angle of the bit, ϕ_j is the friction angle between the bit and rock.

For triangular element $a_1a_2a_3$, the maximum values of the two stress components on the failure plane (σ_{max} and τ_{max} respectively) can be derived as

$$\sigma_{max} = (n+1)\frac{\sin\psi}{z}F_1\cos(\psi+\beta+\phi_j),$$
$$\tau_{max} = -(n+1)\frac{\sin\psi}{z}F_1\sin(\psi+\beta+\phi_j), \tag{2}$$

where n is the distribution coefficient, ψ is the angle between free plane and failure plane, z is the cutting depth (penetration per revolution), and F_1 is the resultant force on the rake surface of the bit.

In Nishimatsu's model, the stress condition of failure of rock is given by an envelope of Mohr's circle of stress, which yields the following:

$$\tau = \frac{1}{2}q_u\frac{1-\sin\phi_i}{\cos\phi_i} + \sigma\tan\phi_i. \tag{3}$$

Therein, σ and τ are the stress components of the failure plane, q_u denotes the unconfined compressive strength of the rock, and ϕ_i is the internal friction angle of the rock.

Inserting Eq. (2) into Eq. (3), the resultant force F_1 can be expressed as shown below

$$F_1 = \frac{1}{2(n+1)}\frac{1-\sin\phi_i}{\sin\psi}\frac{z}{\sin(\psi+\beta+\phi_i+\phi_j)}q_u. \tag{4}$$

In above expression, F_1 varies with ψ. When

$$\frac{\delta F_1}{\delta\psi} = 0,\ \ \psi = \frac{\pi}{2} - \frac{\beta+\phi_i+\phi_j}{2},$$

the minimum value of F_1 is achieved, Eq. (4) can be written as presented below

$$F_1 = \frac{1}{n+1}\frac{1-\sin\phi_i}{1+\cos(\beta+\phi_i+\phi_j)}zq_u. \tag{5}$$

Therefore, the horizontal component P_1 and the vertical component Q_1 can be given as follows:

$$P_1 = k_{1p}zq_u,$$

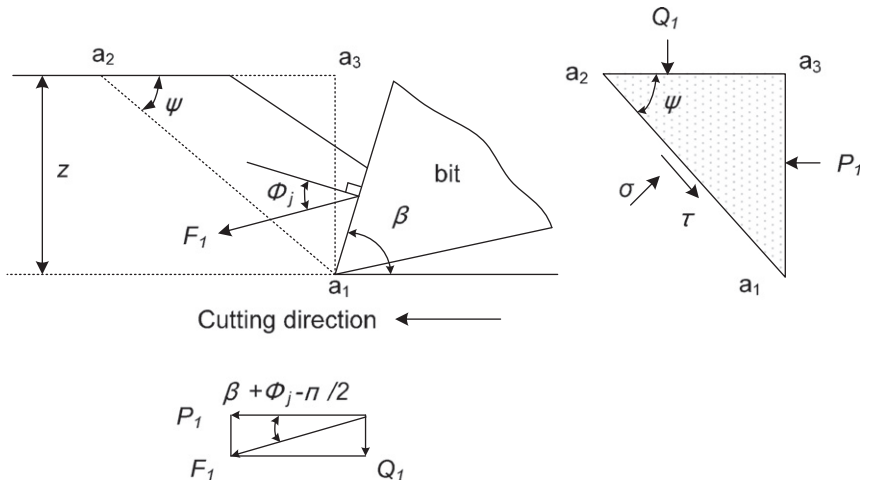

Fig. 2. Geometric and mechanical model for rock cutting (Nishimatsu, 1972).

Table 1
Meanings of signs in Fig. 2.

Sign	Meaning	Sign	Meaning
Φ_j	Friction angle between the bit and rock	F_1	Cutting force
β	Blade angle of the bit	P_1	Main cutting force of F_1 (equivalent to machine torque if consider the distance from the axis)
z	Penetration per revolution	Q_1	Back cutting force of F_1 (equivalent to thrust)
ψ	Angle between free plane and failure plane	σ, τ	Stress components of failure plane

$$Q_1 = k_{1q} z q_u. \tag{6}$$

Therein, the k_{1p}, k_{1q} coefficients are expressible as

$$k_{1p} = \frac{1}{n+1}\frac{(1-\sin\phi_i)\sin(\beta+\phi_j)}{1+\cos(\beta+\phi_i+\phi_j)},$$

$$k_{1q} = \frac{1}{n+1}\frac{(1-\sin\phi_i)\cos(\beta+\phi_j)}{1+\cos(\beta+\phi_i+\phi_j)}.$$

However, this model can not be used to analyze the effects of the wear and friction on the flank surface, since bit wear is not incorporated in Nishimatsu's model. Herein, we attempt to expand and enhance the Nishimatsu theory to fit actual cutting conditions.

Fig. 3 is the modified geometrical and mechanical model for rock cutting. Compared to Fig. 2, a horizontal face is added to the flank surface. In this paper, we call it a *virtual base*. The area of the virtual base represents the degree of bit wear. Generally, a larger contact area engenders heavier bit wear and more intense friction around the blade point.

The static equilibrium in this model is

$$P_c = P_1 + P_2,$$

$$Q_c = Q_1 + Q_2, \tag{7}$$

where P_c and Q_c denote the components of the total cutting force, P_1 and Q_1 denote the components of the cutting force on the rake surface, P_2 and Q_2 are on the flank surface.

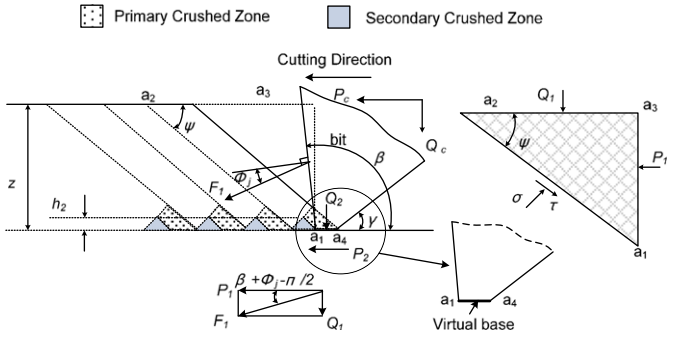

Fig. 3. Modified Nishimatsu's model for rock drilling. A contact surface is added on the bottom of the bit blade. P_c and Q_c are the components of the resultant cutting force.

According to Nishimatsu's theory, a primary crushed zone exists, which is recompacted and stuck to the blade point. Furthermore, after forming of the coarse chip, a secondary crushed zone appears around the blade. Fig. 3 shows the two crushed zones. When considering the influence of the secondary crushed zone, Nishimatsu proposed the following equations:

$$P_c = m_1 + k_{1p} z q_u,$$

$$Q_c = m_2 + k_{1q} z q_u. \tag{8}$$

Therein, m_1 and m_2 are the constants representing the forces generated from the secondary crushed zone.

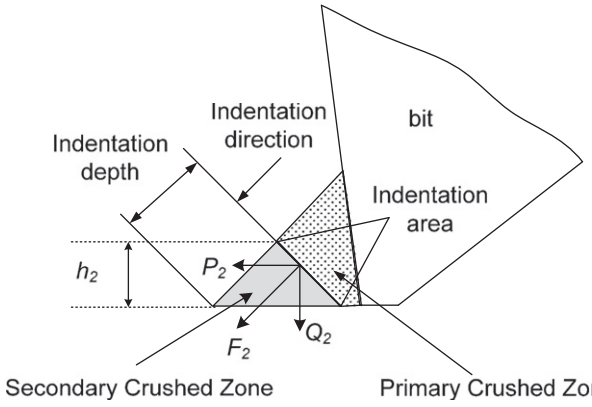

Fig. 4. Primary and secondary crushed zones in drilling processes. The primary crushed zone is stuck on the bit blade and treated as a part of the bit temporarily.

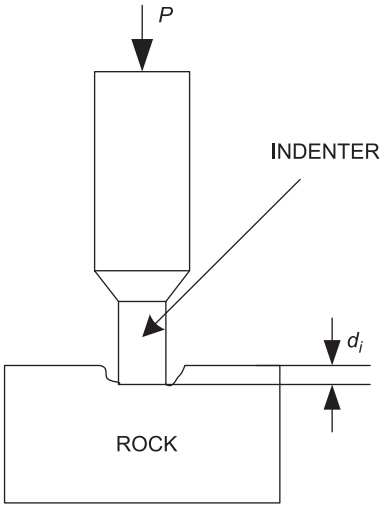

Fig. 5. Mateus et al.'s (2007) indentation model.

Fig. 4 shows that the primary crushed zone is stuck on the bit blade and that it is treated as a temporary part of the bit. The secondary crushed zone is compacted by the primary crushed zone which acts as an indenter. By using an indentation model that will be discussed in the next section (feeding motion), the relation between maximum indentation force F_2 and UCS can be expressed as

$$F_2 = k_{is} q_u, \tag{9}$$

where k_{is} is a coefficient determined by the sizes of the secondary crushed zone and the shape of the built-up edge. The components of F_2 are

$$\begin{aligned} P_2 &= k_{2p} q_u, \\ Q_2 &= k_{2q} q_u, \end{aligned} \tag{10}$$

where k_{2p}, k_{2q} are coefficients.

Clearly, F_2 is the cutting force acting on the blade point to remove the successive secondary crushed zones. Compared with the resultant force F_1 on the rake surface, F_2 is smaller and more constant, even when the cutting depth changes. For convenience, we treat F_2 as acting on the virtual base; P_2 is equivalent to the friction force between the flank surface and the rock. Inserting Eq. (6) and Eq. (10) into Eq. (7), the total horizontal component P_c and the total normal component Q_c of the total resultant cutting force are given as shown below

$$\begin{aligned} P_c &= k_{1p} z q_u + k_{2p} q_u, \\ Q_c &= k_{1q} z q_u + k_{2q} q_u. \end{aligned} \tag{11}$$

Certainly, Eq. (11) is correct only when the cutting depth is greater than the threshold value, which is h_2 in this report. Eq. (11) resembles Eq. (8), but it underscores the influence of UCS on cutting forces.

2.2. Feeding motion

Mateus et al. (2007) used a flat-end indenter to run the indentation tests depicted in Fig. 5. In these tests, the indentation speed was about 0.01 mm/s, with a penetration depth of 0.3 mm. The displacement and load were recorded. The indentation modulus was calculated as

$$IM = \frac{\Delta N}{\Delta d_i}. \tag{12}$$

IM is the indentation modulus (kN/mm); ΔN the change in load (kN); Δd_i the change in indentation (mm).

Meanwhile, the UCS of rock samples was tested. The linear regression between indentation modulus IM and UCS was made as the following equation:

$$q_u = k_m IM, \tag{13}$$

K_m is the coefficient (17.38 MPa × mm/kN).

This equation shows a proportional relation between UCS and IM. The unit of IM is kN/mm. We believe that a parameter with a unit of MPa/mm is more rational to define the effect of the indentation by an indenter. In Mateus's tests, the flat end of the indenter is a 1-mm-diameter cylinder. We define parameter indentation strength (IS) to describe the resistance of a rock to indentation

$$IS = \frac{\Delta P}{\Delta d_i}, \tag{14}$$

IS is the indentation strength (MPa/mm); ΔP the change in pressure (MPa).

Eq. (13) can be rewritten to represent the relation between IS and UCS as shown below

$$q_u = k_I IS, \tag{15}$$

k_I is the coefficient (0.0546 mm).

Next we apply this equation to the drilling process presented in Fig. 1. Here, s and h are the step length and indentation depth of a drilling cycle, and r is the radius of a point at the bit blade

$$h = \frac{z}{2\pi r/s}. \tag{16}$$

The indentation strength IS of this rock is calculated as

$$IS = \frac{2\pi r Q_f}{bzs}. \tag{17}$$

Therein, Q_f denotes the load for indentation, and b represents the contact length of the flank surface in the cutting direction. Considering the difference between indentation tests and drilling processes, the relation between indentation strength and UCS can be written as shown below

$$q_u = k_{i0} IS, \tag{18}$$

k_{i0} is the coefficient.

Inversely, we can evaluate the feeding (indentation) force Q_f with the following equation:

$$Q_f = \frac{k_{it} bzs}{2\pi r} q_u. \tag{19}$$

Therein, k_{it} is a coefficient. Furthermore, we have the expression presented below

$$P_f = Q_f \tan\phi_j = \frac{k_{it} bzs \tan\phi_j}{2\pi r} q_u, \tag{20}$$

here, P_f denotes the friction force resulting from the indentation of the bit.

2.3. Cutting forces and drilling specific energy

We analyzed drilling processes by regarding one drilling cycle, for convenience, as two steps: indentation and cutting. However, it is more rational to regard the two steps as occurring simultaneously when we consider the maximum cutting force in actual drilling. The total circumferential force P can be expressed as presented below

$$P = P_1 + P_2 + P_f. \tag{21}$$

The total torque T is

$$T = \int_{r_1}^{r_2} Pr dr + T_i, \tag{22}$$

where T_i is the torque generated from the idle running of a drill, and where r_1 and r_2 are the inner and outer radii of the bit.

Therefore, torque can be presented as the following expression:

$$T = k_c z q_u + k_r b q_u + k_f bz q_u + T_i, \tag{23}$$

where

$$k_c = \frac{(r_2^2 - r_1^2)}{2(n+1)} \frac{(1-\sin\phi_i)\sin(\beta+\phi_j)}{1+\cos(\beta+\phi_i+\phi_j)},$$

$$k_r = \frac{(r_2{}^2 - r_1{}^2)}{2(n+1)} \frac{(1-\sin\phi_i)\sin\beta\sin\phi_j}{1+\cos(\beta+\phi_i+\phi_j)},$$

$$k_f = \frac{k_{it} s \tan\phi_j (r_2 - r_1)}{2\pi}$$

are coefficients depending on the bit shapes and the rock properties. Eq. (23) shows that the total drilling torque comprises four parts: cutting torque, friction torque on the flank surface of the bit, feeding (or indentation) torque, and idle running torque. The first term on the right is the torque caused by cutting, which is proportional to the cutting depth z, the penetration per revolution. The second term results from the friction on the bit flank surface when the indentation process is not considered. The third term is the torque attributable to the feeding motion (indentation), proportional to the product of the cutting depth z and the length of the virtual base b. The fourth term, T_i, is a constant for a drill.

According to Eq. (23), the total torque consists of two parts: effective torque and ineffective torque. Effective torque is the sum of the first term (cutting) and the third (feeding). It is the necessary torque to form and remove rock chips in the drilling processes. Effective torque Te can be presented as the following expression:

$$Te = \int_{r_1}^{r_2} (P_1 + P_f) r dr \tag{24}$$

The sum of the second term (friction) and the fourth (idle running) is the ineffective torque, which is best eliminated or reduced.

Teale (1965) proposed a concept naming specific energy, and found that the UCS of rocks is comparable to the minimum specific energy. Other researchers also verified the relation between specific energy and rock strengths (Li et al., 2009; Hoberock and Bratcher, 1996; Balci et al., 2004; Tiryaki and Dikmen, 2006; Basarir et al., 2008; Scoble et al., 1989). Specific energy has been accepted as an important parameter to evaluate rock properties.

According to Teale, the specific energy is defined as the amount of work necessary for the removal of a unit volume of rock. The specific energy can be expressed as shown below

$$Es = \frac{F}{A} + \frac{2\pi T}{Az}. \tag{25}$$

Therein, Es denotes the specific energy, F is the thrust, T is the torque, and A is the effective cross-sectional area of the hole. Here, *effective cross-sectional area* means the area of the circular loop formed by the outer and inner radii of a bit.

Investigations showed that the value of the second term is about 10–200 times greater than the first in Eq. (25) (Li, 2011). Energy resulting from torque is the main part of the drilling specific energy. Therefore, we have the following when the energy resulting from thrust is neglected

$$Es = \frac{2\pi T}{Az}. \tag{26}$$

Inserting Eq. (23) into Eq. (26), we obtain

$$Es = \frac{2\pi}{A}\left(\frac{k_r b q_u + T_i}{z} + k_c q_u + k_f b q_u\right). \tag{27}$$

This equation shows that the drilling specific energy Es is inversely proportional to the cutting depth z.

And, effective specific energy is defined as shown below

$$Ees = \frac{2\pi Te}{Az}. \tag{28}$$

Clearly, the relation between effective specific energy and *UCS* can be expressed as the following equation:

$$Ees = \frac{2\pi}{A}(k_c q_u + k_f b q_u), \tag{29}$$

where *Ees* is the effective specific energy. The right-hand-side of Eq. (29) does not include z, the cutting depth. It contains only the effective part of the specific energy in the drilling process: the specific energy consumed by cutting and feeding and that by friction on the flank surface and idle running were removed. Therefore, effective specific energy is more reasonable than total specific energy when evaluating the drilling efficiency or predicting the *UCS* of rocks from drilling data.

3. Laboratory and field experiments

3.1. Laboratory experiments

(1) Experimental equipment.

Several experiments were performed in our laboratory to verify the proposed model. An MWD system was used for this research, as depicted in Fig. 6. The hardware consists of a bench drilling machine, four sensors to detect and record mechanical data (torque, thrust, rotational speed and stroke), and a data-logger. Signals from these sensors were amplified through an amplifier circuit and were shown and recorded on a computer with a sampling time of 100 ms.

An application software was developed to analyze the data recorded by this MWD. First, useless data (idle running, ceasing, etc.) are removed, only drilling data are retained. Second, time-serial data are converted to depth-serial data at regular intervals. In this step, the average values of data at 1 mm intervals were calculated not only for the original data, i.e. torque, thrust, rotational speed and stroke, but also for some necessary derived parameters including torque/thrust, bit penetration per revolution, and specific energy.

As portrayed in Fig. 7, a two-wing bit (outer diameter 28 mm) was used in this research. To investigate the effects of bit wear, the bit blades were made flat-ended. The reshaped plane width was treated as the contact length b. Four types of materials were chosen: brick, gypsum, cement, and sulfide ore rock.

(2) Relation between *UCS* and torque(penetration rate).

Eq. (23) shows the complex relation between torque, rock properties, bit shape and wear, and penetrations rate. Because the first three items are proportional to *UCS*, the slopes of the terms in penetration rate–torque graph can be interpreted as rock types if the bit shape and wear are constant. Several drilling tests were conducted on materials of those four types to verify the relation between *UCS* and torque. A new bit was used to avoid the influence of bit wear. The rotary speed was set in 580 r/min. Mechanical data were recorded and analyzed according to the procedure presented above. A penetration rate–torque graph was created to show the results in Fig. 8. The slope changes can be explained as the differences of *UCS*.

Table 2 shows data obtained from experiments using a new bit. Each intercept in this table is ineffective torque for the equivalent material. Ineffective torque is also linear to *UCS*.

(3) Influence of contact length b on torque.

The third term in Eq. (23) contains the product of b and d, which means that the bit wear can also engender some differences in the slopes, even for same rocks and same bits. Fig. 9 shows different slopes when using the same bit, but the wear degree of the bit blade was changed intentionally (b=0.1, 0.5, 1.0 mm). It verified the influence of the contact length of the virtual base on the drilling torque, just as shown in Eq. (23).

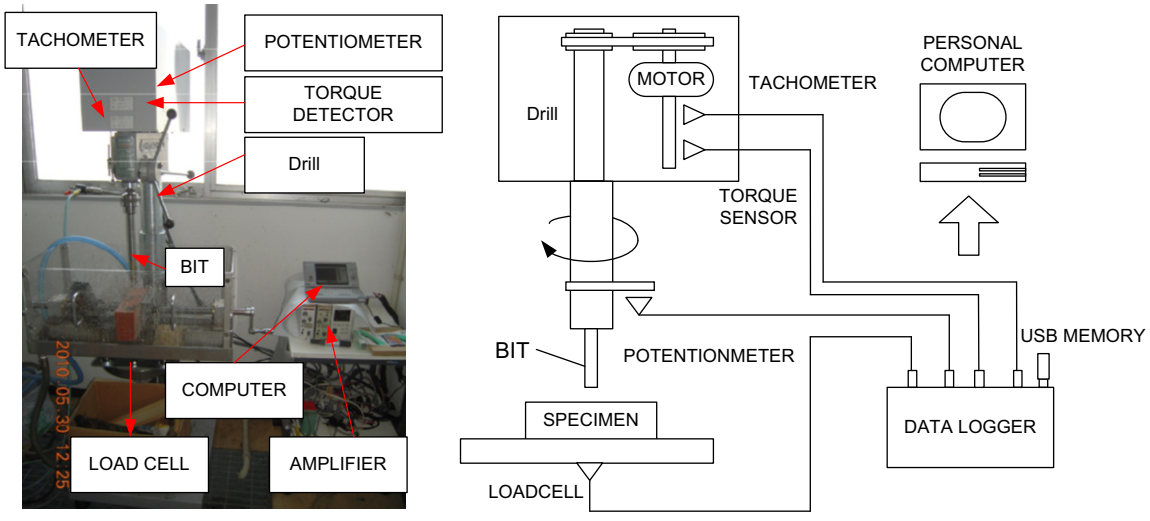

Fig. 6. MWD in the laboratory experiments.

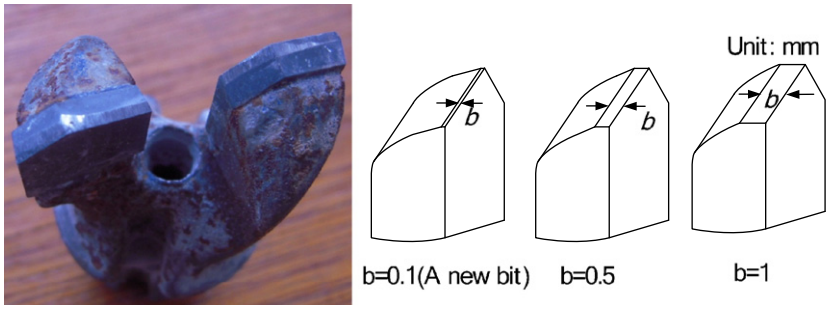

Fig. 7. Two-wing bit and its reshaping.

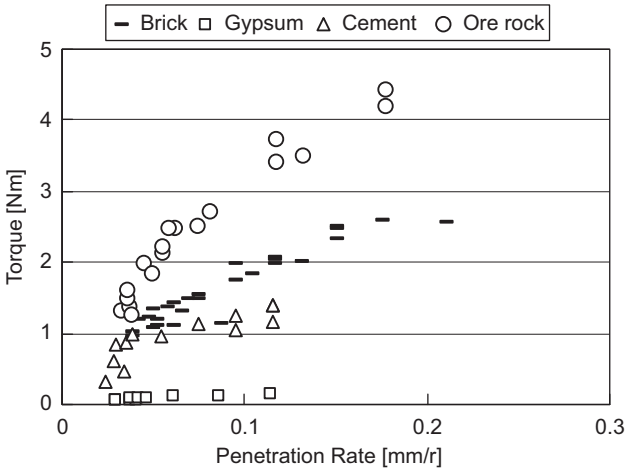

Fig. 8. Relation between torque and penetration rate.

Table 2
Slopes and intercepts of the penetration rate–torque lines.

Material	*UCS* (MPa)	Slope	Intercept
Gypsum	0.3	0.9087	0.037
Cement	6.5	7.7979	0.444
Brick	12	10.803	0.665
Sulfide ore	20	20.398	0.906

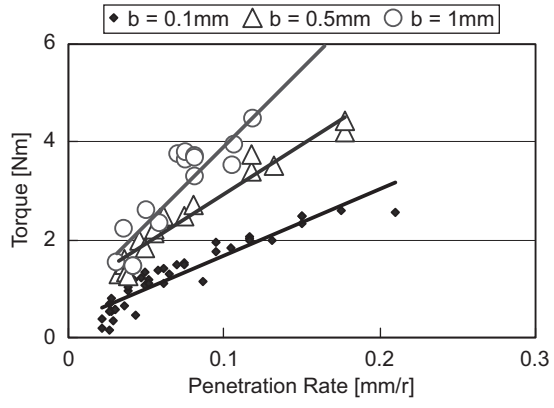

Fig. 9. Contact length and penetration rate–torque relation.

(4) Effective specific energy.

Specific energy is calculable using Eq. (26). The effective specific energy must be calculated using the effective torque. For each type of these materials, the effective torque equals the result of subtracting the intercept from the total torque.

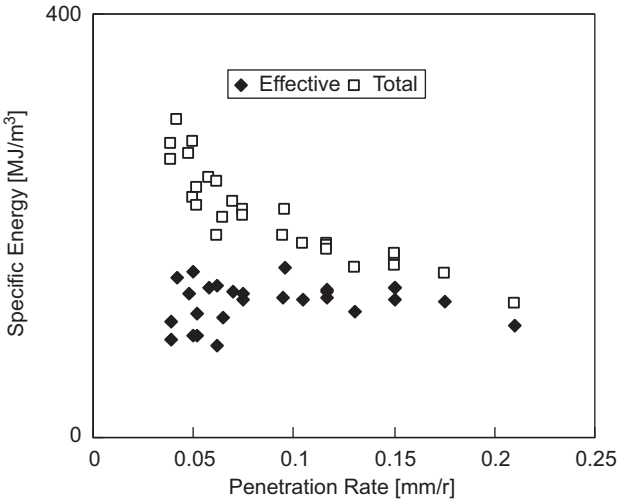

Fig. 10. Specific energy and effective specific energy (laboratory experiments).

Fig. 10 shows a comparison between specific energy and effective specific energy of drilling on the brick. Both change with *UCS*. The specific energy is inversely proportional to the penetration rate whereas effective specific energy is independent from it. Other types of materials show similar trends. Therefore, effective specific energy is a better index for evaluating the *UCS* of rocks. This figure also verified the correctness of the proposed model.

3.2. Field experiments

(1) Experiment devices.

An MWD system developed by Itakura et al. (2008) was modified to drill in the field. The drilling machine was a Trussmaster 1 P/N TRUSS001-1828. Table 3 shows the specifications of this machine and the concept diagram of this drilling machine is shown in Fig. 11. A photo taken while drilling is shown in Fig. 12.

This drilling machine is provided with detachable wheels for easy mobility. The stinger secures the machine during drilling. Four sensors were used to detect the drilling data including torque, thrust, rotational speed and stroke.

The signals from these sensors were amplified through an *IS* barrier amplifier circuit. Then they were recorded on a USB memory with a sampling time of 10 or 100 ms.

As was the case with the laboratory drilling system, the software developed by Trussmaster can analyze the drilling data and calculate necessary parameters including torque/thrust, bit penetration per revolution, specific energy, and effective specific energy. Additionally, the locations of discontinuities, rock types, or *UCS* can be predicted using the analyzed data. The predicted results are shown as a 2D or 3D image of the geostructure using a VRML.

(2) Effective specific energy and *UCS*.

A field experiment was performed at the RTV roadway of a coal mine, NSW, Australia (Fig. 13). In addition to 2 boreholes (55-mm-diameter), 47 non-core holes (27 mm, 28 mm, or 55-mm-diameter, 5 m length) were drilled in the roof. Through the drilling processes the drilling data—torque, thrust, rotational speed, and stroke—were measured and recorded. Then the data were analyzed and calculated.

The total drilling specific energy was calculated according to Eq. (26). Fig. 14 shows the relation between specific energy and penetration per revolution for Hole No. 14 as an example. Its specific energy is inversely proportional to the penetration per revolution in the field experiments, just as it is in the laboratory. However, the effective specific energy is difficult to calculate because ineffective torque is not easily differentiated from total torque. Here we use the

Table 3
Performance of the drilling machine (trussmaster).

Item	Capacity	Unit
Revolution	850–900	RPM
Thrust	8.9	kN
Torque	251	N m
Stroke	1.3	m
Air consumption	2832–3398	l/min
Height	1.8–2.8	m
Air pressure	689	kPa

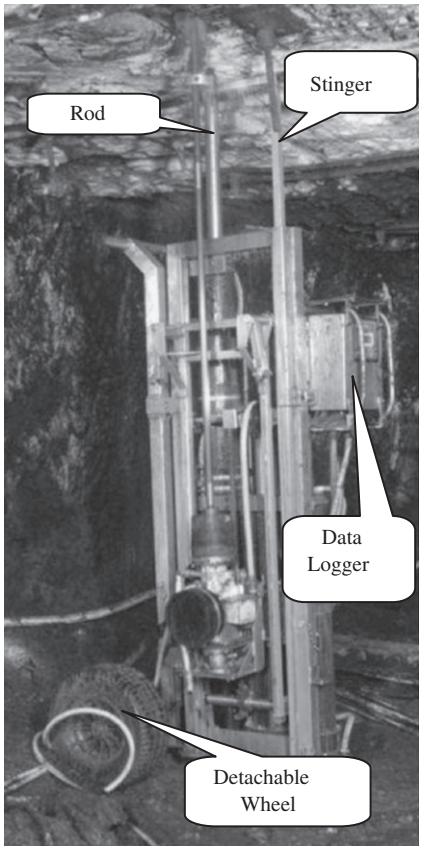

Fig. 12. Trussmaster drilling machine.

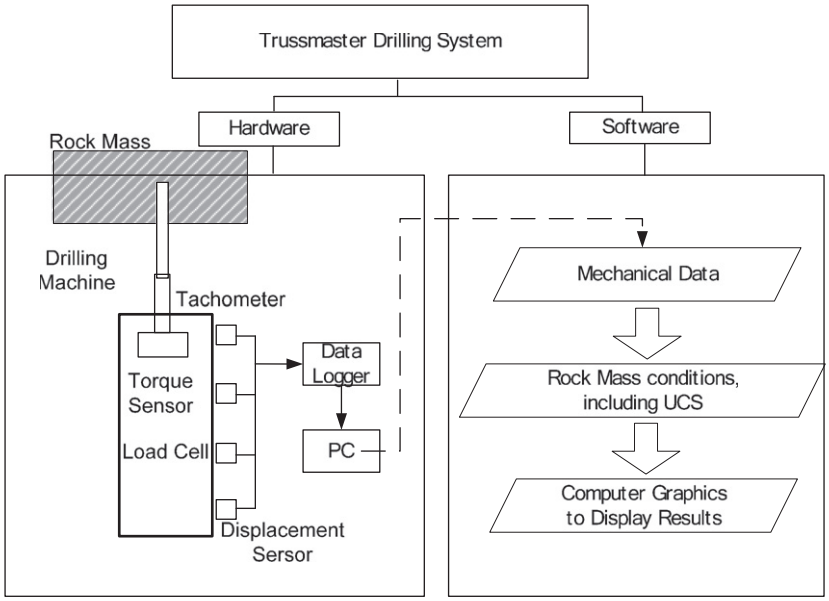

Fig. 11. Concept diagram of Trussmaster drilling system.

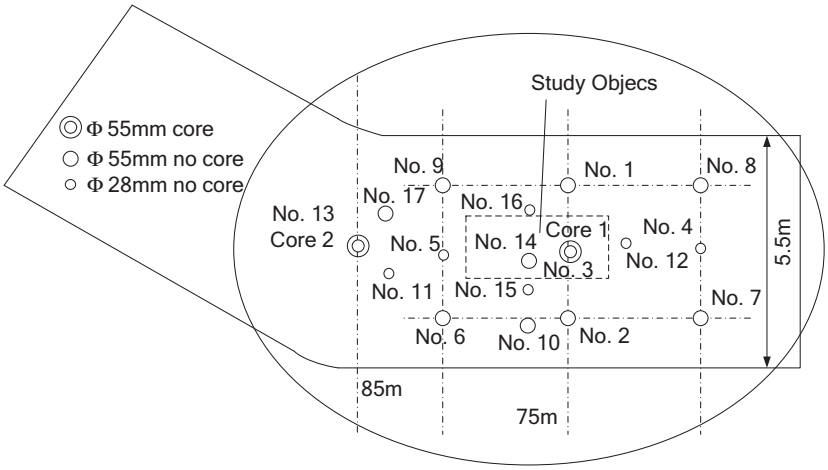

Fig. 13. Layout of the drill holes (plan view of RTV roadway).

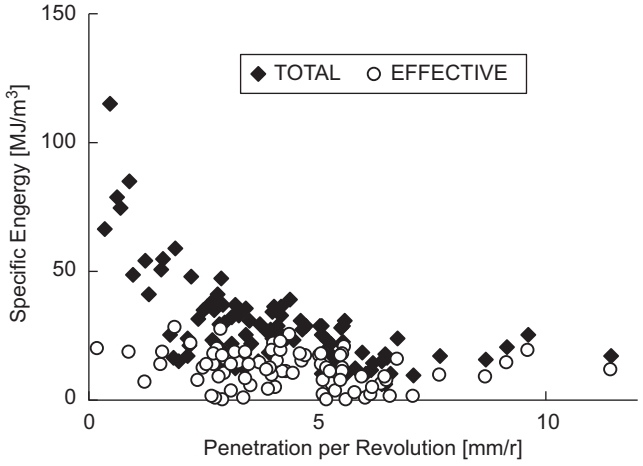

Fig. 14. Total and effective specific energy. The total one is inversely-proportional to the penetration per revolution, whereas the effective one is independent of it (field experiments).

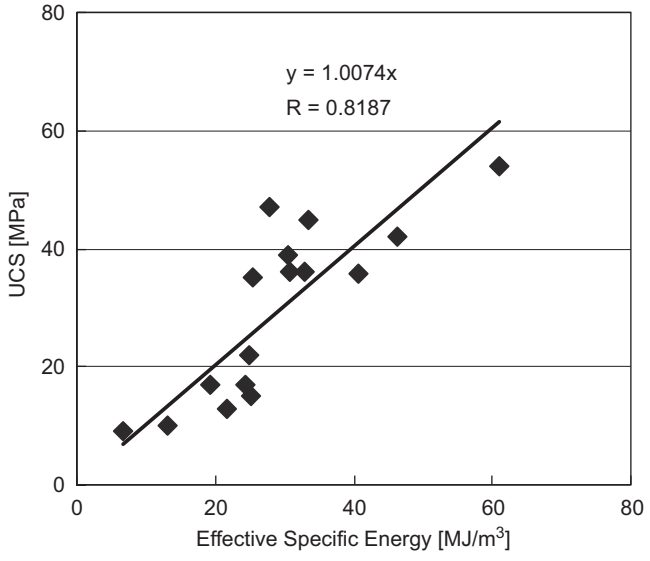

Fig. 15. Proportional relation exists between the drilling specific energy and *UCS*.

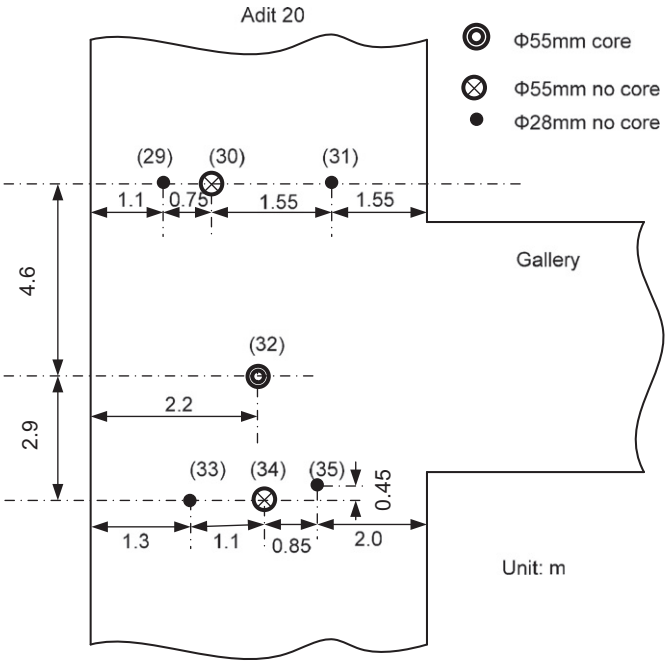

Fig. 16. Layout of the drill holes (plan view of Adit 20 roadway).

torque value corresponding to the minimum penetration per revolution. Fig. 14 also shows the effective specific energy of the same hole. It is independent of the penetration per revolution. Results for other holes show similar trends, just as they do in the laboratory. Therefore, effective specific energy is more reasonable than the total energy when evaluating drilling efficiency or predicting the *UCS* of rocks from field-drilling mechanical data.

To investigate the relationship between effective specific energy and *UCS*, some core specimens were taken from Core 1 (near No. 14 Hole) in the field experiment. In the laboratory, the specimens were tested for measurement of *UCS* in accordance with an established method for confined compression tests

for rocks (Japanese Geotechnical Society, 2000). The proportional relation between the effective specific energy and *UCS* is presented in Fig. 15. This result verifies the correctness of Eq. (29) and suggests a method to predict *UCS* from effective specific energy during drilling. When drilling with the same drilling machines and the same type of bits, under the same drilling conditions, the *UCS* of rocks can be predicted by using the following regressive equation:

$$q_u = Ees. \tag{30}$$

(3) Predicting *UCS* from effective specific energy.

To verify the correctness of the prediction method, we analyzed the data obtained through another on-site experiment, which was conducted at the Adit 20 Roadway, also in Gujarat No. 1 Coal Mine, Australia. Fig. 16 depicts a detailed plan of this site. The type of bits and drilling conditions were the same as those used at the RTV Roadway. We selected a core hole (No. 32) and a non-core hole (No. 29) as the research objects. The test for the *UCS* of rocks from the core was performed. The mechanical data of No. 34 Hole were analyzed, the effective specific energy was calculated, and the *UCS* was evaluated according to Eq. (30).

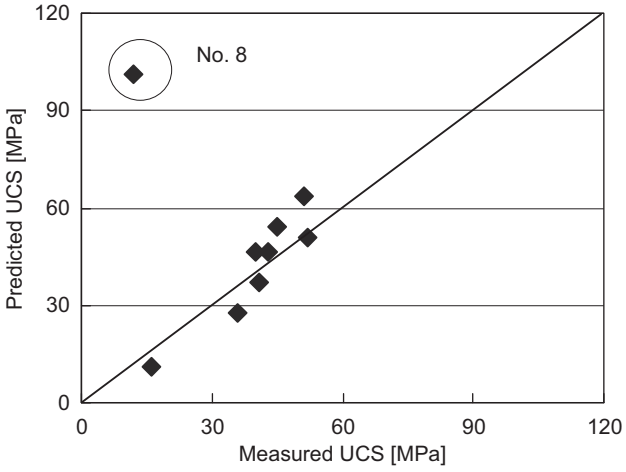

Fig. 17. Predicted and measured values of *UCS*.

The relation between the measured values and predicted values of the *UCS* is presented in Fig. 17. It is apparent that, for most samples, the prediction is successful with an acceptable accuracy. On the other hand, the prediction for sample No. 8 was not good. A possible reason is that large quantities of rock waste, water, and clay may have clogged the drill bit, in effect increasing the specific energy considerably even though the rock was soft.

At last, the predicted *UCS* was displayed in a virtual space as shown in Fig. 18. This enables the operators understand the 3D geostructure of the roadway intuitively.

4. Conclusions

We developed an analytical model for rotary drilling by using drag bits. In this model, a drilling process consisted of successive cycles, each of which contains feeding and cutting. Nishimatsu's rock cutting theory was used to analyze rock cutting with flat bits. Feeding motion was regarded as an indentation with a bit. This drilling model for flat bits integrates Nishimatsu's rock cutting model with Mateus's indentation model.

For fitting drilling processes, a virtual base at the flank surface is added to Nishimatsu's model to represent bit wear and friction at the bit flank surface. The resistance force resulting from the secondary crushed zone was analyzed as acting on the virtual base of a bit.

Mateus's indentation model shows that indentation force is proportional to the product of the penetration depth per revolution and the area of the virtual base, when the *UCS* of the rock is constant. Therefore, a larger virtual

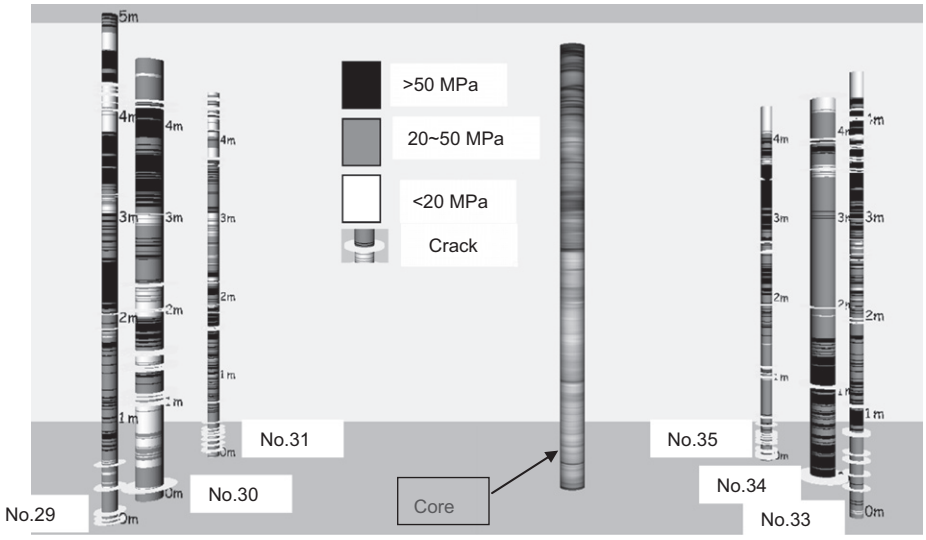

Fig. 18. Visualization of the predicted *UCS* of the rocks along Adit 20 roadway.

base engenders greater energy consumption for intense wear of a bit.

The total drilling torque is resolved into four parts generated respectively from cutting, friction on the flank surface, feeding, and idle running. The cutting and feeding torque, which are proportional to the penetration depth per revolution, are the effective part of the total torque. The effective specific energy is calculable using the effective torque. Theoretical analyses showed that effective specific energy does not vary with the penetration depth per revolution if the *UCS* of a rock is constant. This engenders a promising method for evaluating *UCS* of rocks from effective specific energy.

Laboratory and field experiments were conducted. They verified the correctness of the proposed model. They also verified that *UCS* of rocks can be evaluated from effective specific energy with acceptable accuracy.

Acknowledgments

Field experiments in this research were supported by Japan Coal Research Centre (JCOAL) and Rambor Ltd., Australia. The authors would like to thank them for their contributions.

References

Balci, C., Demircin, M.A., Copur, H., Tuncdemir, H., 2004. Estimation of optimum specific energy based on rock properties for assessment of roadheader performance. Journal of the South African Institute of Mining and Metallurgy 104 (11), 633–643.

Basarir, H., Karpuz, C., Tutluoglu, L., 2008. Specific energy based rippability classification system for coal measure rock. Journal of Terramechanics 45 (1–2), 45–52.

Beattie, N.C.M., 2009. Monitoring-While-Drilling for Open-Pit Mining in a Hard Rock Environment: An Investigation of Pattern Recognition Techniques Applied to Rock Identification. Master's Thesis. Queen's University.

Deketh, H.J.R., 1995. Wear of rock cutting tools, laboratory experiments on the abrasivity of rock. Balkema, Rotterdam.

Detournay, E., Defourny, P., 1992. A phenomenological model of the drilling action of drag bits. International Journal of Rock Mechanics and Mining Sciences and Geomechanics Abstracts 29, 13–23.

Detournay, E., Richard, T., Shepherd, M., 2008. Drilling response of drag bits: theory and experiment. International Journal of Rock Mechanics and Mining Sciences and Geomechanics Abstracts 45, 1347–1360.

Evans, I., 1962. A theory on the basic mechanics of coal ploughing. In: Proceedings of International Symposium on Mining Research, vol. 2. London, pp. 761–798.

Finfinger, G., Peng, S.S., Gu, Q., Wilson, G., Thomas, B., 2000. An approach to identify geological properties from roof bolter drilling parameters. In: Proceedings of the 19th Conference on Ground Control in Mining, pp. 1–11.

Goktan, R.M., 1997. A suggested improvement on Evans' cutting theory for conical bits. In: Proceedings of the Fourth International Symposium on Mine Mechanization Automation, vol. 1 (A4). Brisbane, Australia, pp. 57–61.

Gunes, Y.N., Yurdakul, M., Goktan, R.M., 2007. Prediction of radial bit cutting force in high-strength rocks using multiple linear regression analysis. International Journal of Rock Mechanics and Mining Sciences 44 (6), 962–970.

Hoberock, L.L., Bratcher, G.J., 1996. A new approach for determining in-situ rock strength while drilling. Journal of Energy Resources Technology 118 (4), 249–255.

Itakura, K., Goto, T., Yoshida, Y., Tomita, S., Iguchi, S., Ichihara, Y., Mastalir, P., 2008. Portable intelligent drilling machine for visualizing roof-rock geostructure. In: Proceedings of Aachen International Mining Symposia—Rockbolting in Mining and Injection Technology and Roadway Support Systems, pp. 597–609.

Kahraman, S., Bilgin, N., Ferindunoglu, C., 2003. Dominant rock properties affecting the penetration rate of percussive drills. International Journal of Rock Mechanics and Mining Sciences 40 (5), 711–723.

LaBelle, D., Bares, J., Nourbakhsh, I., 2000. Material classification by drilling. In: Proceedings of the 17th International Symposium on Automation and Robotics Construction. September, Taipei, Taiwan, pp. 1–6.

Li, Z., Itakura, K., Tomita, S., Iguchi, S., Ichihara, Y., Mastalir, P., 2009. Prediction of rock strength from rotary drill performance parameters. In: Proceedings of 2009 Korea–Japan Joint Symposium on Rock Engineering. Suwon, Korea, pp. 57–65.

Li, Z., 2011. Research on the Prediction of Roof Geostructure using Drilling Mechanical Data. Doctoral Thesis. Muroran Institute of Technology.

Martin, J., 2007. Application of Pattern Recognition Techniques to Monitoring While-Drilling on a Rotary Electric Blast Hole Drill at an Open-Pit Coal Mine. Master's Thesis. Queen's University.

Mateus, J., Saavedra, N.F., Carrillo, Z.C., Mateus, D., 2007. Correlation development between indentation parameters and unconfined compressive strength for Colombian sandstones. Ciencia, Tecnología y Futuro 3 (3), 125–135.

Merchant, M.E., 1945. Basic mechanics of the metal cutting process. Journal of Applied Physics 66, 168–175.

Nakajima, I., Kinoshita, S., 1979. Theoretical studies on cutting force of rock fracture mechanism in rock cutting. Journal of the Mining and Metallurgical Institute of Japan 95 (1092), 49–55.

Nishimatsu, Y., 1972. The mechanics of rock cutting. International Journal of Rock Mechanics and Mining Sciences and Geomechanics Abstracts 9, 261–270.

Okubo, S., Fukui, K., Chen, W., 2010. Size and shape of TBM debris estimated by the Nishimatsu's cutting-resistance equation. Journal of MMIJ 126, 24–30.

Rojek, J., 2007. Discrete element modelling of rock cutting. Computer Methods in Materials Science 7 (2), 224–230.

Roxborough, F.F., Philips, H.R., 1975. Rock excavation by disc cutter. International Journal of Rock Mechanics and Mining Sciences and Geomechanics Abstracts 12, 361–366.

Scoble, M.J., Peck, J., Hendricks, C., 1989. Correlation between rotary drill performance parameters and borehole geophysical logging. Mining Science and Technology 8, 301–312.

Su, O., Akcin, N.A., 2009. Numerical simulation of rock cuttability. In: Kulatilake, P.H.S.W. (Ed.), Proceedings of the International Conference on Rock Joints and Jointed Rock Masses. Paper 1111. Kulatilake and Associates, Tucson, Arizona, USA.

Teale, R., 1965. The concept of specific energy in rock drilling. International Journal of Rock Mechanics and Mining Sciences and Geomechanics Abstracts 2, 57–73.

The Japanese Geotechnical Society, 2000. JGS2521-2000 (Method for Confined Compression Test for Rocks). Available from 〈http://www.jiban.or.jp/organi/bu/kijyunbu/kouji/200807/JGS_252〉.

Tiryaki, B., Dikmen., A.C., 2006. Effects of rock properties on specific cutting energy in linear cutting of sandstones by picks. Rock Mechanics and Rock Engineering 39 (2), 89–120.

Utt, W.K., 1999. Neural network technology for strata strength characterization. In: Proceedings of International Joint Conference on Neural Networks, vol. 6, Washington, DC, USA, pp. 3806–3809.